Macromolecules

pubs.acs.org/Macromolecules
Article

Reaction-Induced Miscibility in Styrene- and Benzoxazine-Based Copolymers with Poly(vinylpyrrolidone) Blends Through Strong Intermolecular Hydrogen-Bonding Interactions

Tzu-Ling Ma, Wei-Ting Du, Yang-Chin Kao, Mohamed Gamal Mohamed, and Shiao-Wei Kuo*

Cite This: Macromolecules 2025, 58, 6215−6227

ABSTRACT: The miscibility behavior of polymer blends has garnered significant interest; however, while most binary polymer blends are immiscible due to thermodynamic challenges, reaction-induced miscibility (RIM) presents a promising yet underexplored phenomenon for achieving homogeneous mixtures through specific intermolecular hydrogen bonding interactions. This study investigates the design and synthesis of novel styrene- and benzoxazine-based copolymers to achieve RIM behavior with a poly(vinylpyrrolidone) (PVP) homopolymer. Two benzoxazine monomers, HPMI-BZ and Ty-BZ, were synthesized via Mannich condensation, incorporating maleimide groups to enable free radical copolymerization with styrene monomer to form PS-*alt*-P(HPMI-BZ) and PS-*alt*-P(Ty-BZ) alternating copolymers, which were characterized using Fourier-transform infrared (FTIR) spectroscopy, nuclear magnetic resonance (NMR) spectroscopy, matrix-assisted laser desorption/ionization time-of-flight (MALDI-TOF) mass spectrometry, differential scanning calorimetry (DSC), and thermogravimetric analysis (TGA). The thermal and miscibility behaviors of the PS-*alt*-P(HPMI-BZ)/PVP and PS-*alt*-P(Ty-BZ)/PVP binary blends were analyzed, focusing on their intermolecular hydrogen bonding after thermal ring-opening polymerization (ROP). Results demonstrated that the incorporation of functional groups such as OH units from benzoxazine units through thermal ROP facilitated strong intermolecular interactions with the C═O units of PVP, enabling RIM in otherwise immiscible blends. This work highlights the interplay between molecular structure, thermal stability, and miscibility behavior, offering insights into the development of next-generation thermoset/thermoplastic materials with tailored properties.

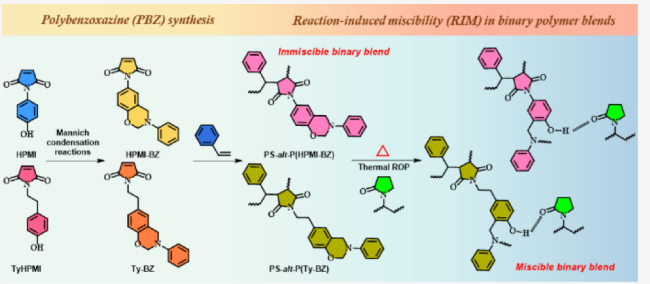

INTRODUCTION

The miscibility behavior of polymer blends has received significant interest during the last four decades because of their potential applications in coatings and adhesives,[1,2] biomedical applications,[3] and high-performance materials such as in aerospace and electronics.[4,5] However, most binary polymer blends are immiscible due to the unique thermodynamic properties of high molecular weight with low entropy of mixing.[6] The long chains of polymers significantly reduce the number of possible configurations upon mixing and result in unfavorable enthalpy of mixing, as polymers usually lack specific intermolecular interactions such as dipole−dipole interactions or hydrogen bonding.[7−9] To enhance miscibility behavior, intermolecular hydrogen bonding has been utilized in binary blends, which results in a homogeneous mixture of two or more polymers that mix at the molecular scale, forming a single-phase system.[10−12] Unlike immiscible polymer blends, which exhibit phase separation with two glass transition temperature (T_g) values, miscible blends exhibit a single T_g value and uniform physical properties.[13,14]

The other famous polymer blends were also widely investigated in thermoset/thermoplastic blends during the thermal curing process of the thermoset matrix.[15,16] The reaction-induced phase separation (RIPS) mechanism has been identified to explain the interplay of thermal curing or polymerization, phase behavior, and thermodynamics, leading to the formation of distinct morphologies.[17] In general, the thermoset prepolymer and thermoplastic components are usually miscible at the start of the process because of their compatibility in the uncured state. As thermal polymerization progresses, the molecular weight of the thermoset increases, reducing its miscibility with the thermoplastic, and these changes destabilize the initially homogeneous mixtures. The reduction in miscibility promotes phase separation, where the thermoplastic components phase separate into distinct domains within the thermal curing thermoset matrix, which has potential applications in improving fracture toughness by

Received: January 1, 2025
Revised: April 17, 2025
Accepted: June 2, 2025
Published: June 11, 2025

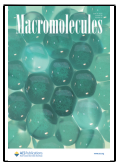

https://doi.org/10.1021/acs.macromol.5c00004
Macromolecules 2025, 58, 6215−6227

absorbing energy during crack propagation and optimized mechanical or thermal properties.[18] RIPS in thermoset/thermoplastic blends is a complex process influenced by thermodynamics, kinetics, and material properties.

In this work, we are interested in reaction-induced miscibility (RIM) in polymer blends, which is an intriguing but less common phenomenon compared to RIPS.[19] Most thermal curing in polymer blend systems drives phase separation because of the incompatibilities arising during polymerization or curing by increasing the molecular weight of polymers that unfavorably drive the entropy term of Gibbs free energy. As a result, RIM requires strong specific interactions, which could generate new functional groups that increase intermolecular interactions between polymers after thermal polymerization.[20] In previous works,[19−21] the reaction creates covalent bonds between the two polymers, such as transesterification between an acid and alcohol in the polymer blend system, or the reaction between an epoxy resin and a functionalized thermoplastic, which can form a miscible system during thermal curing if grafting or cross-linking occurs at the interface by covalent bonds.[21−23] The presence of functional groups such as hydroxyl (OH), carboxyl (COOH), or amine units after thermal polymerization of the thermoset matrix can form strong intermolecular hydrogen bonding with thermoplastic from an immiscible polymer blend; however, forming a miscible polymer blend in such cases is rare.

Herein, we carefully design the polymer blend system involving polybenzoxazine (PBZ) mixed with the typical strong hydrogen bonding acceptor, poly(vinylpyrrolidone) (PVP) homopolymer. Polybenzoxazines, a class of thermosetting polymers, have garnered significant attention in recent years because of their remarkable thermal stability,[24] mechanical strength,[25] and tunable surface properties,[26,27] making them ideal candidates for advanced material applications such as coatings, adhesives, flame retardants,[28,29] and high-performance nanocomposites.[30−32] These unique properties arise from the thermal ring-opening polymerization (ROP) of benzoxazine monomers, which facilitates the formation of highly cross-linked network structures because of their strong intramolecular and intermolecular hydrogen bonding.[33−37] The immiscible PS/PVP binary blend has been widely investigated because PS is a hydrophobic polymer and PVP is a hydrophilic polymer.[38,39] To enhance the miscibility behavior of PS/PVP binary blends, the incorporation of the strong hydrogen-bonded donor segment of poly(vinylphenol) (PVPh) into the PS segment of PS-*co*-PVPh random copolymers to form strong intermolecular hydrogen bonding interactions between the C═O units of PVP and the OH units of PVPh has been widely discussed.[7,10] The predicted phase diagram of these copolymer/homopolymer systems can usually be determined by the Painter-Coleman Association Model (PCAM),[10] where the interassociation equilibrium constant (K_A) of the PVPh/PVP binary blend (K_A = 6000) is stronger than the self-association equilibrium constant (K_B) of the pure PVPh homopolymer (K_B = 66.8).[10,40]

To obtain reaction-induced miscibility (RIM) in immiscible PS/PVP binary blends, the benzoxazine monomer should copolymerize with the styrene monomer to form PS-*co*-PBZ copolymers through free radical copolymerization. In this work, we aim to address these challenges by synthesizing two novel hydroxyphenylmaleimide-based benzoxazine monomers, HPMI-BZ and Ty-BZ, through Mannich condensation reactions. These monomers incorporate maleimide functional groups, which are known to enhance cross-linking density and thermal performance. We further extend the utility of these monomers by copolymerizing them with the styrene monomer to form alternating copolymers PS-*alt*-P(HPMI-BZ) and PS-*alt*-P(Ty-BZ). The design and synthesis of these materials are intended to explore the interplay between molecular structure, thermal stability, and their potential for RIM behavior with the PVP homopolymer upon thermal ROP.

To confirm the chemical structures and assess the thermal properties of the synthesized HPMI-BZ and Ty-BZ monomers and PS-*alt*-P(HPMI-BZ) and PS-*alt*-P(Ty-BZ) copolymers, we employed a comprehensive suite of characterization techniques, including NMR, FTIR, DSC, TGA, and MALDI-TOF mass spectrometry. The miscibility behavior and intermolecular hydrogen bonding behavior of PS-*alt*-P(HPMI-BZ)/PVP or PS-*alt*-P(Ty-BZ)/PVP blends were characterized by using DSC thermal analyses and 1D and 2D-FTIR spectra. This work not only introduces novel monomers and copolymers with enhanced thermal properties through thermal ROP but also provides a deeper understanding of RIM behavior, paving the way for the development of next-generation thermoset/thermoplastic blends.

EXPERIMENTAL SECTION

Materials. Aniline (99.5%), xylene, ethyl acetate (EA), dichloromethane (DCM), toluene, and methanol (MeOH) were supplied by Acros Organics. Tetrahydrofuran (THF), *N*,*N*-dimethylformamide (DMF), and 1,4-dioxane were obtained from Sigma-Aldrich. Paraformaldehyde (98%), PVP (M_n = 58 000 g/mol), and styrene (99%) were acquired from Alfa Aesar. Azobis(isobutyronitrile) (AIBN), chlorobenzene, magnesium sulfate anhydrous ($MgSO_4$, 99%), and sodium hydroxide (NaOH, 97%) were purchased from SHOWA. All chemicals were used without further purification. The hydroxyphenylmaleimide (HPMI) and *N*-(ethyl-4-hydroxyphenyl)maleimide (TyHPMI) monomers were synthesized by our group previously.[41,42]

The Synthesis of HPMI-BZ Monomer. HPMI monomer (0.567 g, 3 mmol) and paraformaldehyde (0.198 g, 6.6 mmol) were placed in a 100-mL round-bottomed flask, and the cosolvent mixture of xylene (4.5 mL) and chlorobenzene (10.5 mL) was added to the flask. Subsequently, aniline (273 μL, 3 mmol) was added, and the mixture was heated to 120 °C until a homogeneous solution was obtained, then refluxed for 24 h. After being cooled to ambient temperature, the solution was concentrated under vacuum to remove most of the solvent and then dissolved in DCM (30 mL). The organic phase was extracted three times with 1 M NaOH, followed by water, to remove any residue. The organic layer was dried over $MgSO_4$ and concentrated using a rotary evaporator to yield an earthy-yellow gel. The synthesis method used is similar to that described in the referenced procedure.[43−45] [Yield: 71%; mp 111 °C; exothermic curing peak 225 °C]; FTIR (KBr, cm^{-1}): 1713 (C═O), 1598 (C═C), 934 (oxazine ring); ^{1}H NMR (500 MHz, DMSO−d_6, δ, ppm): 4.70 (s, 2H, Ar−C**H**$_2$N), 5.50 (s, 2H, O−C**H**$_2$N), 6.82−7.07, 7.24 (m, 8H, Ar−**H**), 7.14 (s, 2H, C**H**═C**H**); ^{13}C NMR (125 MHz, DMSO−d_6, δ, ppm): 48.86 (Ar−**C**H$_2$N), 78.83 (O−**C**H$_2$N), 116.52−129.12 (aromatic **C**), 123.79 (**C**−CH$_2$−N of oxazine ring), 134.54 (**C**H═**C**H), 147.59 (aromatic **C**−N), 153.39 (**C**−O−CH$_2$ of oxazine ring), and 170.12 (**C**═O).

The Synthesis of Ty-BZ Monomer. Similar to the procedure for HPMI-BZ, TyHPMI monomer (0.260 g, 1.2

https://doi.org/10.1021/acs.macromol.5c00004
Macromolecules 2025, 58, 6215−6227

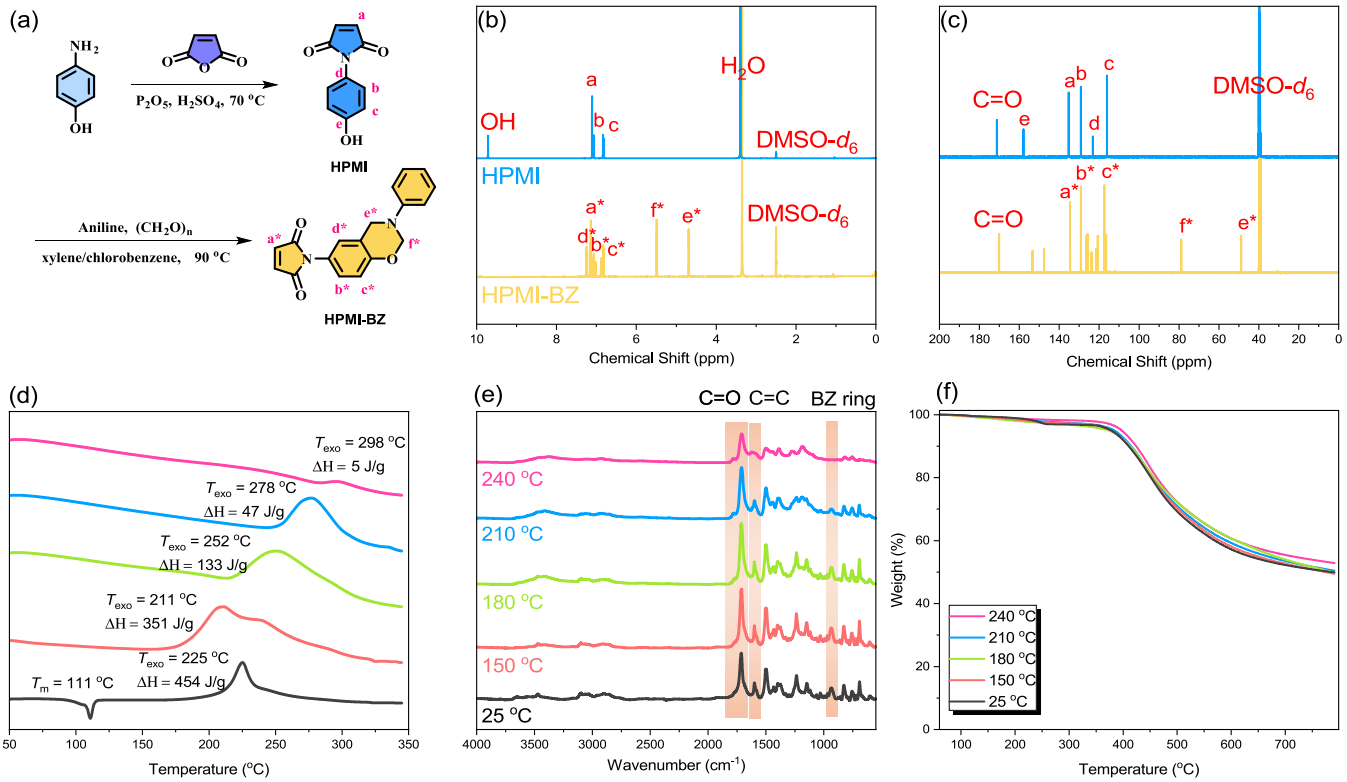

Figure 1. (a) The synthesis of the HPMI-BZ monomer from the HPMI monomer, and their corresponding (b) ^{1}H NMR, (c) ^{13}C NMR, (d–f) DSC, FTIR, and TGA analyses of the HPMI-BZ monomer under various thermal ROP temperature procedures.

mmol) and paraformaldehyde (0.075 g, 2.5 mmol) were placed in a 100-mL round–bottom flask, and a cosolvent mixture of xylene (8 mL) and chlorobenzene (8 mL) was added. Aniline (108 μL, 1.2 mmol) was added subsequently, and the mixture was heated to 120 °C until a homogeneous solution was achieved, followed by refluxing for 24 h under a N_2 atmosphere. After cooling to ambient temperature, the solution was concentrated under vacuum to yield a gel–like product, which was then dissolved in EA (30 mL). The organic phase was extracted three times with 0.5 M NaOH and then with water to remove any residual impurities. Finally, the organic layer was dried over $MgSO_4$ and concentrated using a rotary evaporator to obtain a burnt–orange solid. [Yield: 51%; mp 125 °C; exothermic curing peak 243 °C]; FTIR (KBr, cm^{-1}): 1709 (C═O), 1599 (C═C), 949 (oxazine ring); ^{1}H NMR (500 MHz, DMSO–d_6, δ, ppm): 2.69 (t, 2H, Ar–C**H**$_2$), 3.57 (t, 2H, Mal–C**H**$_2$), 4.59 (s, 2H, Ar–C**H**$_2$N), 5.40 (s, 2H, O–C**H**$_2$N), 6.61–6.92, 7.09–7.22 (m, 8H, Ar–**H**), 6.98 (s, 2H, C**H**=C**H**); ^{13}C NMR (125 MHz, DMSO–d_6, δ, ppm): 32.93 (**C**H$_2$–CH$_2$), 48.67 (Ar–**C**H$_2$N), 78.81 (O–**C**H$_2$N), 116.12–129.92 (aromatic **C**), 121.09 (**C**–CH$_2$–N of oxazine ring), 134.43 (**C**H═**C**H), 147.80 (aromatic **C**–N), 152.48 (**C**–O–CH$_2$ of oxazine ring), and 170.80 (**C**═O).

The Synthesis of PS-*alt*-Poly(HPMI-BZ) and PS-*alt*-Poly(Ty-BZ) Copolymers. In a 50-mL two-necked round-bottom flask, HPMI-BZ (0.872 g, 2.85 mmol), TyBZ (1.00 g, 3.00 mmol), and AIBN (5 wt %) were placed, and the system was subjected to a vacuum/N_2 cycle. Dry THF (20 mL) was then injected to achieve a homogeneous solution, followed by the addition of styrene (0.33 mL, 2.85 mmol for HPMI-BZ or 0.34 mL, 3.00 mmol for TyBZ). The reaction mixture underwent three freeze–pump–thaw/N_2 cycles to remove dissolved gases. Subsequently, the mixture was stirred under a N_2 atmosphere at 70 °C for 24 h. The reaction was quenched by exposing the solution to air for an hour and concentrated using rotary evaporation to remove most of the solvent. The crude product was then poured into a large amount of cold MeOH, and the solid was reprecipitated multiple times from cold THF/MeOH. The final product was dried under high vacuum at 40 °C for 2 days to remove any residual solvent. For the PS-*alt*-Poly(HPMI-BZ) copolymer: FTIR (KBr, cm^{-1}): 1713 (C═O), 934 (oxazine ring); ^{1}H NMR (500 MHz, DMSO–d_6, δ, ppm): 4.59 (s, 2H, Ar–C**H**$_2$N), 5.44 (s, 2H, O–C**H**$_2$N), 6.31–7.60 (m, 13H, Ar**H**); ^{13}C NMR (125 MHz, DMSO–d_6, δ, ppm): 48.88 (Ar–**C**H$_2$N), 79.07 (O–**C**H$_2$N), 117.51–129.41 (aromatic **C**), 121.52 (**C**–CH$_2$–N of oxazine ring), 134.43 (**C**H═**C**H), 147.65 (aromatic **C**–N), 153.90 (**C**–O–CH$_2$ of oxazine ring), 177.80 (**C**═O); GPC was measured using a THF system (M_n = 4480 g/mol and PDI = 1.43, Figure S1a). For PS–*alt*–Poly(Ty-BZ) copolymer: FTIR (KBr, cm^{-1}): 1700 (C═O), 947 (oxazine ring); ^{1}H NMR (500 MHz, DMSO–d_6, δ, ppm): 4.54 (s, 2H, Ar–C**H**$_2$N), 5.36 (s, 2H, O–C**H**$_2$N), 6.21–7.80 (m, 13H, Ar**H**); ^{13}C NMR (125 MHz, DMSO–d_6, δ, ppm): 32.21 (**C**H$_2$–CH$_2$), 49.06 (Ar–**C**H$_2$N), 78.91 (O–**C**H$_2$N), 117.51–129.41 (aromatic **C**), 120.75 (**C**–CH$_2$–N of oxazine ring), 134.43 (**C**H═**C**H), 147.95 (aromatic **C**–N), 152.70 (**C**–O–CH$_2$ of oxazine ring), 177.97 (**C**═O); GPC was measured using a THF system (M_n = 4210 g/mol and PDI = 1.69, Figure S1b).

PS-*alt*-P(HPMI-Bz)/PVP and PS-*alt*-P(Ty-BZ)/PVP Binary Blends. Binary blends of PS-*alt*-P(HPMI-BZ)/PVP and PS-*alt*-P(Ty-BZ)/PVP were prepared using the solution-casting method with a 5 wt % polymer composition. The polymers were dissolved in a cosolvent mixture of DMF/toluene/1,4-dioxane and stirred overnight until a homogeneous solution was obtained. The resulting blends were then

https://doi.org/10.1021/acs.macromol.5c00004
Macromolecules 2025, 58, 6215–6227

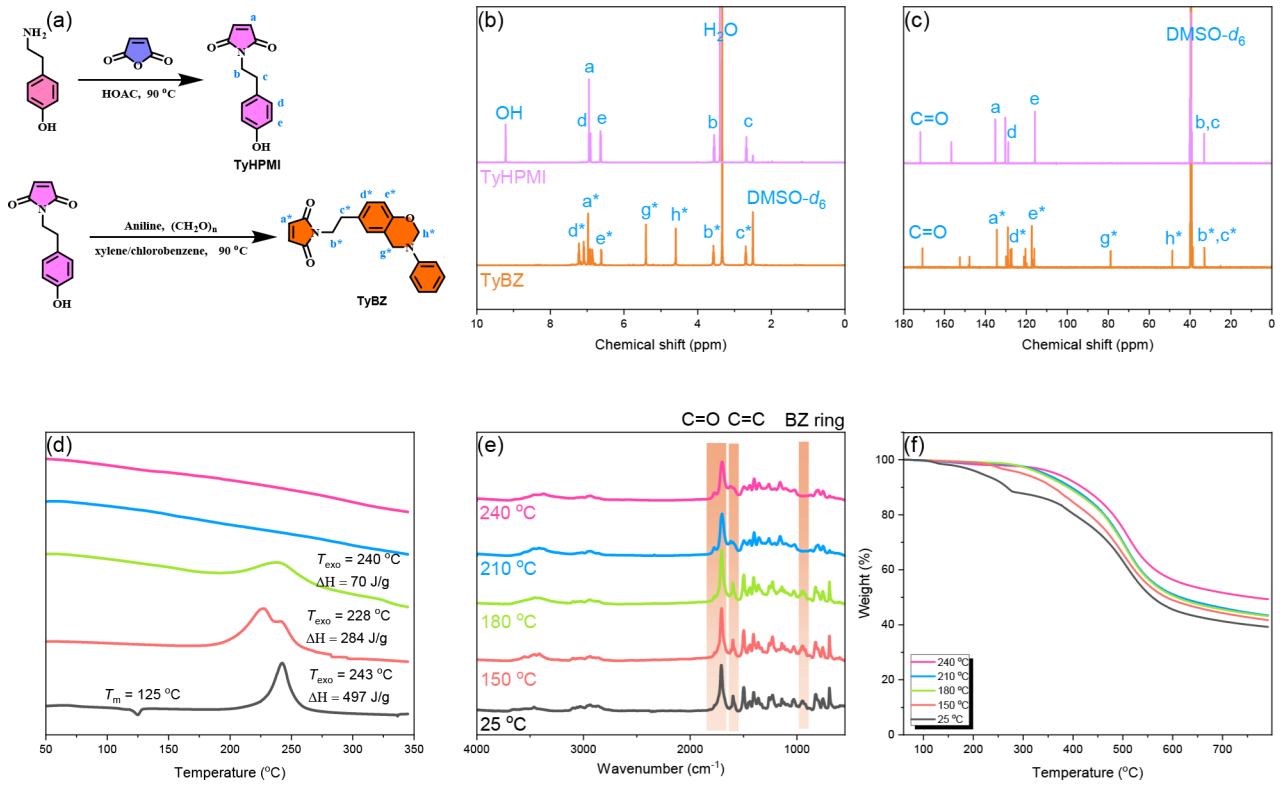

Figure 2. (a) The synthesis of the Ty-BZ monomer from the TyHPMI monomer, and their corresponding (b) ^{1}H NMR, (c) ^{13}C NMR, (d–f) DSC, FTIR, and TGA analyses of the Ty-BZ monomer under various thermal ROP temperature procedures.

placed in a fume hood until most of the solvent had evaporated, after which they were transferred to a vacuum oven at ambient temperature and left for 1 week to ensure the complete removal of any residual solvent.

Thermal Polymerization of HPMI-BZ and Ty-BZ Monomers or PS-*alt*-poly(HPMI-BZ) and PS-*alt*-poly-(Ty-BZ) Copolymers. During the thermal treatment, varying weights of HPMI-BZ and Ty-BZ monomers or PS-*alt*-poly(HPMI-BZ) and PS-*alt*-poly(Ty-BZ) copolymers were subjected to temperatures ranging from 150 to 240 °C for 2 h. Consequently, each sample transitioned in color from an orange to a black solid.

RESULTS AND DISCUSSION

Synthesis and Characterization of HPMI-BZ and Ty-BZ Monomers. The HPMI-BZ and Ty-BZ monomers were synthesized through a Mannich condensation reaction by using HPMI (or TyHPMI), aniline, and $(CH_2O)_n$ as summarized in Figures 1a and 2a. The chemical structures of these two newly synthesized benzoxazine monomers were characterized by using ^{1}H and ^{13}C NMR, DSC, FTIR, and TGA analyses, as displayed in Figures 1 and 2. Figure 1b displays ^{1}H NMR spectra of HPMI and the formation of the benzoxazine ring of the HPMI-BZ monomer, which appeared at 4.70 ppm (*e*) and 5.50 ppm (*f*) due to the Ar−**CH$_2$**−N and O−**CH$_2$**−N units. In addition, the OH unit of HPMI at 9.71 ppm disappeared, and the aromatic protons were located at 7.24−6.80 ppm after the formation of the HPMI-BZ monomer. In Figure 1c, the ^{13}C NMR spectra of the HPMI-BZ monomer exhibited signals at 48.86, 78.83, and 170.12 ppm, corresponding to the Ar−**C**H$_2$N (*e*), O-**C**H$_2$N (*f*), and **C**=O groups, respectively. The FTIR absorption peaks at 1713 cm^{-1}, 1598 cm^{-1}, and 934 cm^{-1} in Figure 1e recorded at room temperature, corresponded to C=O, C=C, and the oxazine ring of the HPMI-BZ monomer, respectively. Furthermore, the integral area ratio of Ar−**CH$_2$**−N and O−**CH$_2$**−N was approximately 1:1, indicating the high purity of the HPMI-BZ monomer. The melting point was observed at 111 °C in Figure 1d (black line), with thermal ROP occurring at 225 °C and an enthalpy of 454 J/g. Figure 1d–f presents the DSC thermograms, FTIR spectra, and TGA analyses, respectively, of the HPMI-BZ monomer under various thermal ROP conditions. As the thermal ROP temperature increased from 25 to 150 °C, the melting point disappeared, and the thermal ROP peak of the BZ ring shifted to a lower temperature at 211 °C with an enthalpy of 351 J/g, as displayed in Figure 1d. When the ROP temperature was further increased from 150 to 240 °C, the thermal ROP peaks shifted to higher temperatures, and the enthalpy further decreased before completely disappearing at 240 °C, suggesting the formation of a highly cross-linked poly-(HPMI-BZ) network. It also displays the T_g behavior at 267 °C, which is significantly higher than the typical Pa-type benzoxazine (180 °C)[30] due to the extra cross-linking density from the maleimide (C=C) unit after thermal ROP. Concurrently, Figure 1e displayed that the absorption bands of the C=C unit at 1598 cm^{-1} and the oxazine ring at 934 cm^{-1} were diminished as the thermal ROP temperature rose from 25 to 210 °C and completely disappeared after 240 °C, consistent with the DSC analyses (Figure 1d). In addition, the C=O unit of HPMI at 1713 cm^{-1} shifted to 1706 cm^{-1} and became broader, indicating intermolecular hydrogen bonding of C=O---HO after thermal ROP. Figure 1f shows TGA analyses, indicating that the HPMI-BZ monomer with T_{d5} (temperature at 5% weight loss) of 377 °C and a char yield of 49.9 wt %. Following thermal ROP at 240 °C, the T_{d5} values moderately increased to 397 °C, with corresponding char

https://doi.org/10.1021/acs.macromol.5c00004
Macromolecules 2025, 58, 6215−6227

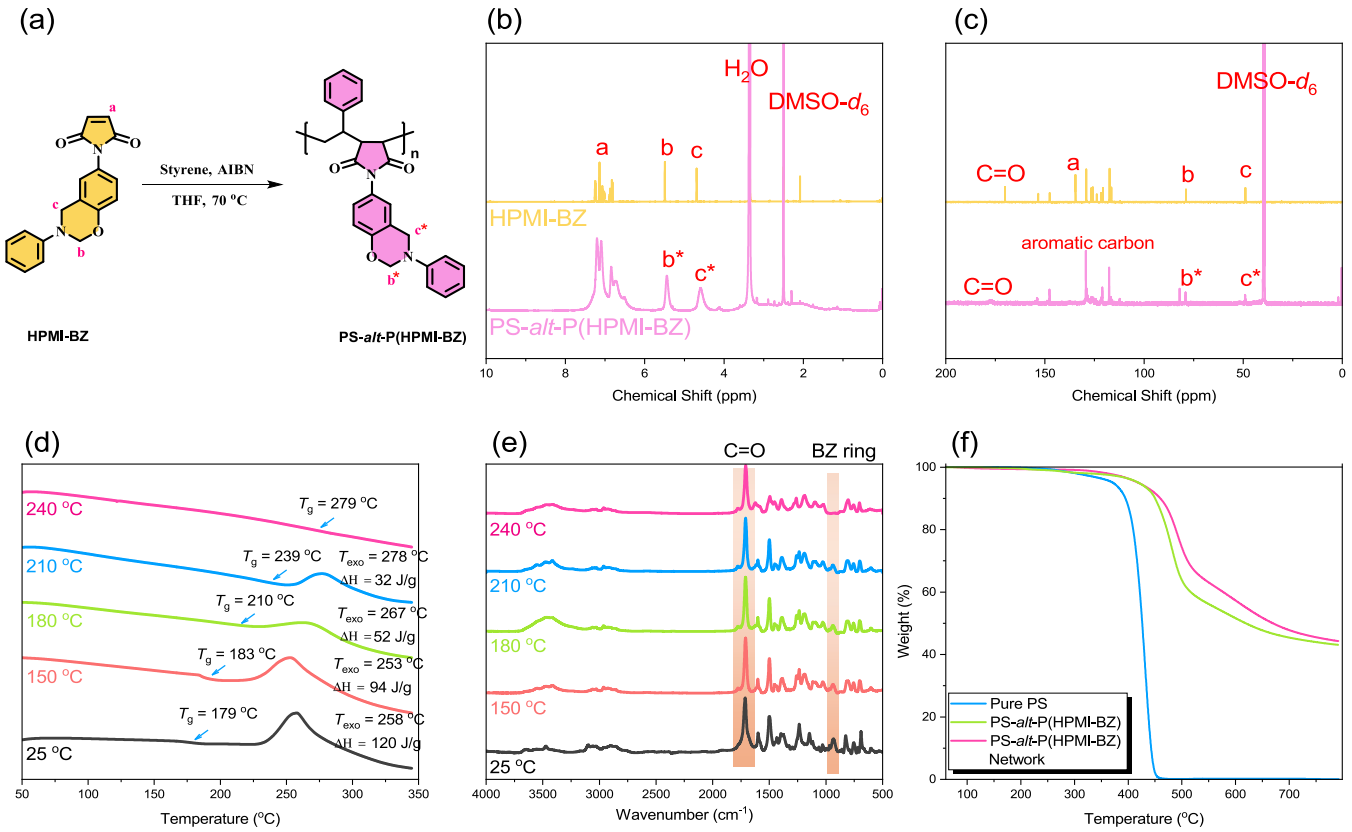

Figure 3. (a) The synthesis of the PS-*alt*-P(HPMI-BZ) copolymer by free radical copolymerization from styrene and the HPMI-BZ monomer, and their corresponding (b) ^{1}H NMR, (c) ^{13}C NMR, (d–e) DSC and FTIR analyses under various thermal ROP temperature conditions, and (f) TGA analyses of pure PS, PS-*alt*-P(HPMI-BZ) copolymer, and PS-*alt*-P(HPMI-BZ) network.

yields of 52.9 wt %, further confirming the formation of the poly(HPMI-BZ) network.

Similar to the HPMI-BZ monomer, Figure 2b presents ^{1}H NMR spectra of TyHPMI and Ty-BZ after the formation of the benzoxazine ring, observed at 4.59 ppm (*h*) and 5.40 ppm (*g*), corresponding to the Ar−**CH$_2$**−N and O−**CH$_2$**−N units. The OH unit of TyHPMI at 9.23 ppm also vanished, while the aromatic protons were located at 7.22–6.60 ppm, and the methylene units of Ty-BZ remained at 2.69 ppm (Ar−C**H$_2$**) and 3.57 ppm (N−C**H$_2$**) after the formation of the Ty-BZ monomer. ^{13}C NMR spectra of the Ty-BZ monomer in Figure 2c exhibited signals at 48.67, 78.81, 170.80, and 32.93 ppm, corresponding to the Ar−**C**H$_2$N (e), O−**C**H$_2$N (f), **C**=O, and Ar−**C**H$_2$ groups, respectively. Figure 2e displays the FTIR spectra of the Ty-BZ monomer recorded at room temperature, showing absorption bands at 1709 cm^{-1} due to the C=O stretching, 1599 cm^{-1} due to C=C stretching, and 949 cm^{-1} corresponding to the oxazine ring, indicating the successful formation of the Ty-BZ monomer by FTIR and NMR analyses. Figure 2d shows the DSC analyses of the Ty-BZ monomer under various thermal ROP conditions, which exhibited a melting temperature at 125 °C and a thermal ROP peak at 243 °C with an enthalpy of 497 J/g, indicating the high purity of the Ty-BZ monomer (black line), which is confirmed by the integral area ratio of Ar−**CH$_2$**−N and O−**CH$_2$**−N of approximately 1:1 by the NMR analysis in Figure 2b. Figure 2d–f presents the DSC thermograms, FTIR spectra, and TGA analyses, respectively, of the Ty-BZ monomer under varying thermal ROP conditions. As the thermal ROP temperature increased from 25 to 150 °C, the melting point disappeared, and the thermal ROP peak of the BZ ring shifted to a lower temperature at 228 °C with an enthalpy of 284 J/g, as shown in Figure 2d. Upon further increasing the ROP temperature from 150 to 240 °C, the thermal ROP peaks shifted to higher temperatures, while the enthalpy gradually decreased and eventually vanished at 210 and 240 °C, indicating the formation of a highly cross-linked poly(Ty-BZ) network. Figure 2e highlights that the absorption bands corresponding to the C=C unit at 1599 cm^{-1} and the oxazine ring at 949 cm^{-1} diminished as the thermal ROP temperature rose from 25 to 180 °C and completely disappeared after 210 °C, aligning with the DSC results (Figure 2d). Moreover, the C=O band of Ty-MI shifted from 1709 cm^{-1} to 1701 cm^{-1} and became broader, signifying intermolecular hydrogen bonding (C=O---HO) following thermal ROP. Figure 2f presents the TGA analyses, showing that the Ty-BZ monomer exhibited a T_{d5} of 215 °C and a char yield of 39.2 wt %. After thermal ROP at 240 °C, the T_{d5} increased moderately to 365 °C, with the char yield rising to 49.3 wt %, further confirming the formation of the poly(Ty-BZ) network. Clearly, the thermal stability of the poly(Ty-BZ) network is lower than that of the poly(HPMI-BZ) network due to the two extra aliphatic methylene units of Ty-BZ as expected. However, the fraction of intermolecular hydrogen bonding with hydrogen-bonded acceptor units could be increased, as widely investigated in our previous work.[38]

Synthesis of PS-*alt*-P(HPMI-BZ) and PS-*alt*-P(Ty-BZ) Copolymers. The PS-*alt*-P(HPMI-BZ) and PS-*alt*-P(Ty-BZ) copolymers were synthesized through free radical copolymerization by using two previously synthesized benzoxazine

https://doi.org/10.1021/acs.macromol.5c00004
Macromolecules 2025, 58, 6215−6227

monomers with styrene. NMR, FTIR, DSC, and MALDI-TOF mass spectrometry were used to confirm their chemical structures. Figure 3a–c displays the chemical structure, peak assignments, and ^{1}H and ^{13}C NMR spectra of the PS-*alt*-P(HPMI-BZ) copolymer. Two broad peaks observed in the ^{1}H NMR spectrum of PS-*alt*-P(HPMI-BZ) appeared at 4.58 ppm (*c*) and 5.43 ppm (*b*), which are close to the original HPMI-BZ monomer but became broader and shifted upfield due to the strong proton−proton coupling effect on the polymeric chain. Furthermore , the protons on the main chain were located between 1.47 and 3.68 ppm (Figure 3b). The ^{13}C NMR spectrum of PS-*alt*-P (HPMI-BZ) copolymer showed signals at 177.34 and 154.02 ppm, corresponding to the C═O and C−OH units, as displayed in Figure 3c. The C═C unit at 134.25 ppm from the HPMI-BZ monomer disappeared for PS-*alt*-P(HPMI-BZ) copolymer while signals at 48.94 and 79.08 ppm corresponded to the Ar−**C**H$_2$N (*e*) and O−**C**H$_2$N (*f*) units, respectively. Most importantly, the integral area ratio of Ar−**CH$_2$**−N and O−**CH$_2$**−N was approximately 1:1, indicating that the benzoxazine ring did not open during free radical copolymerization with the styrene monomer. The ratio of the HPMI-BZ segment was calculated from peaks *b* and *c* of the oxazine rings compared with the aromatic protons, and the molar percentage of HPMI-BZ was 46.38%.

This value is consistent with an alternating copolymer, which is confirmed by MALDI-TOF mass spectra, shown in Figure 4, revealing evidence of a nearly perfect alternating

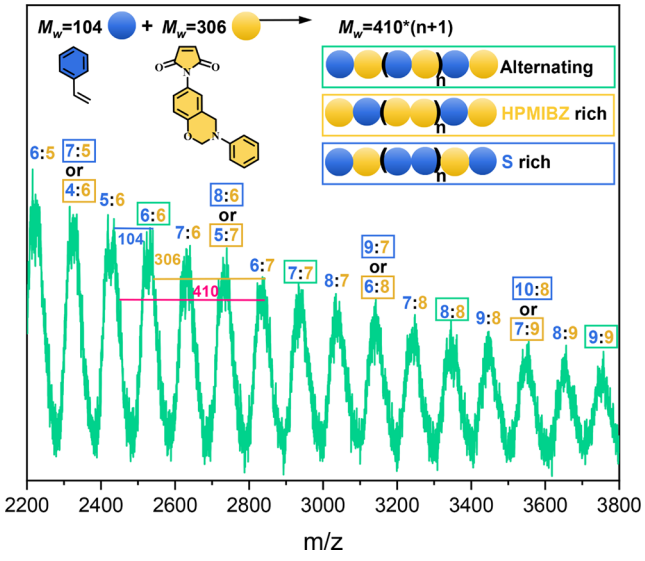

Figure 4. MALDI-TOF mass spectrum of the PS-*alt*-P(HPMI-BZ) copolymer.

copolymer with an equal number of HPMI-BZ and styrene units.[37] For instance, the 410 g mol^{-1} difference between the 1620.10 (HPMI-BZ:S = 4:4) and 2030.2 *m*/*z* (HPMI-BZ:S = 5:5) values is equal to the sum of one HPMI-BZ (306 g mol^{-1}) and one styrene (104 g mol^{-1}) unit of their molecular weights. The nearly perfectly alternating sequences with HPMI-BZ:S ratios of *n* − 1:*n*, *n*:*n*, and *n*:*n* + 1 was also observed in Figure 4.

The thermal ROP behavior of PS-*alt*-P (HPMI-BZ) copolymer was characterized by using DSC and FTIR analyses under various thermal ROP temperatures, as displayed in Figure 3d–e. Pure PS-*alt*-P (HPMI-BZ) copolymer exhibited the thermal ROP peak at 258 °C with an enthalpy of 120 J/g, as shown in Figure 3d, and a T_g behavior at 179 °C, which is significantly higher than that of pure PS (T_g = 100 °C). This behavior is similar to poly(styrene-*alt*-maleic anhydride) (SMA, T_g = 180 °C) without intermolecular hydrogen bonding[37] but much lower than that of pure PS-*alt*-PHPMI copolymer with strong intermolecular hydrogen bonding (T_g = 259 °C).[37] As a result, the PS-*alt*-P(HPMI-BZ) copolymer before thermal ROP reaction, due to the lack of phenolic OH units, would possess the similar T_g behavior to the SMA copolymer. With increasing temperature during thermal treatment, the exothermic peaks shift to relatively lower temperatures from 258 to 253 °C after the thermal ROP procedure at 150 °C, and then shift to relatively higher temperatures of 258 and 278 °C after the thermal ROP procedures at 180 and 210 °C. After the thermal ROP procedure at 240 °C, the exothermic peak and enthalpy nearly vanished, suggesting complete thermal ROP behavior. Furthermore, the T_g behavior increased from 183 to 185, 210, 239, and 279 °C as the thermal ROP temperature from 25 to 240 °C, respectively. Clearly, the T_g value of the PS-*alt*-P(HPMI-BZ) network (T_g = 279 °C) is higher than that of the PS-*alt*-PHPMI copolymer (T_g = 259 °C) because of not only intermolecular hydrogen bonding of OH---OH but also intramolecular hydrogen bonding of OH---N after the formation of the network structure. Figure 3e shows FTIR spectra consistent with the DSC analyses. Clearly, the intensity of the oxazine ring at 934 cm^{-1} of PS-*alt*-P(HPMI-BZ) copolymer decreased as the thermal ROP temperature rose from 25 to 210 °C and completely disappeared after 240 °C. Concurrently, the appearance of the OH units was observed at 3700−2500 cm^{-1} after the thermal ROP, with the main absorptions at 3554 cm^{-1}, 3470 cm^{-1}, 3418 cm^{-1}, and 3240 cm^{-1}, corresponding to free OH, intermolecular OH---OH hydrogen bonding, intermolecular OH---O═C, and intramolecular OH---N hydrogen bonding, respectively.[30] Furthermore, the C═O unit of PS-*alt*-P(HPMI-BZ) copolymer shifted from 1712 cm^{-1} to 1709 cm^{-1} and became broader, indicating intermolecular hydrogen bonding of C═O---HO after thermal ROP, forming the PS-*alt*-P (HPMI-BZ) network. Figure 3f displays the TGA analyses of pure PS, PS-*alt*-P(HPMI-BZ) copolymer, and PS-*alt*-P(HPMI-BZ) network after thermal ROP at 240 °C, indicating that pure PS exhibited a T_{d5} value of 371 °C and a char yield of 0.1 wt %. PS-*alt*-P(HPMI-BZ) copolymer exhibited the T_{d5} value increased moderately to 420 °C, with the char yield rising to 43.1 wt %, which is slightly higher than that of PS-*alt*-PHPMI copolymer (T_{d5} = 417 °C and char yield = 13.8 wt %) as expected. After thermal ROP at 240 °C, the T_{d5} value slightly increased to 421 °C, with the char yield rising to 44.3 wt %, further confirming the formation of the PS-*alt*-P(HPMI-BZ) network. To the best of our knowledge, this is the first work on benzoxazine-functional PS synthesized through free radical copolymerization to improve the thermal properties of the PS segment through thermal ROP.

Figure 5a–c presents the chemical structure, peak assignment, and ^{1}H and ^{13}C NMR of PS-*alt*-P(Ty-BZ) copolymer. Similarly, two broad peaks were observed at 5.34 ppm (*b*) and 4.50 ppm (*c*) in the ^{1}H NMR spectrum of PS-*alt*-P (Ty-BZ) copolymer, which are not only close to the original Ty-BZ monomer but also shift upfield due to the strong proton−proton coupling effect on the polymeric chain, as shown in Figure 5b. Figure 5c presents ^{13}C NMR spectrum of PS-*alt*-

https://doi.org/10.1021/acs.macromol.5c00004
Macromolecules 2025, 58, 6215−6227

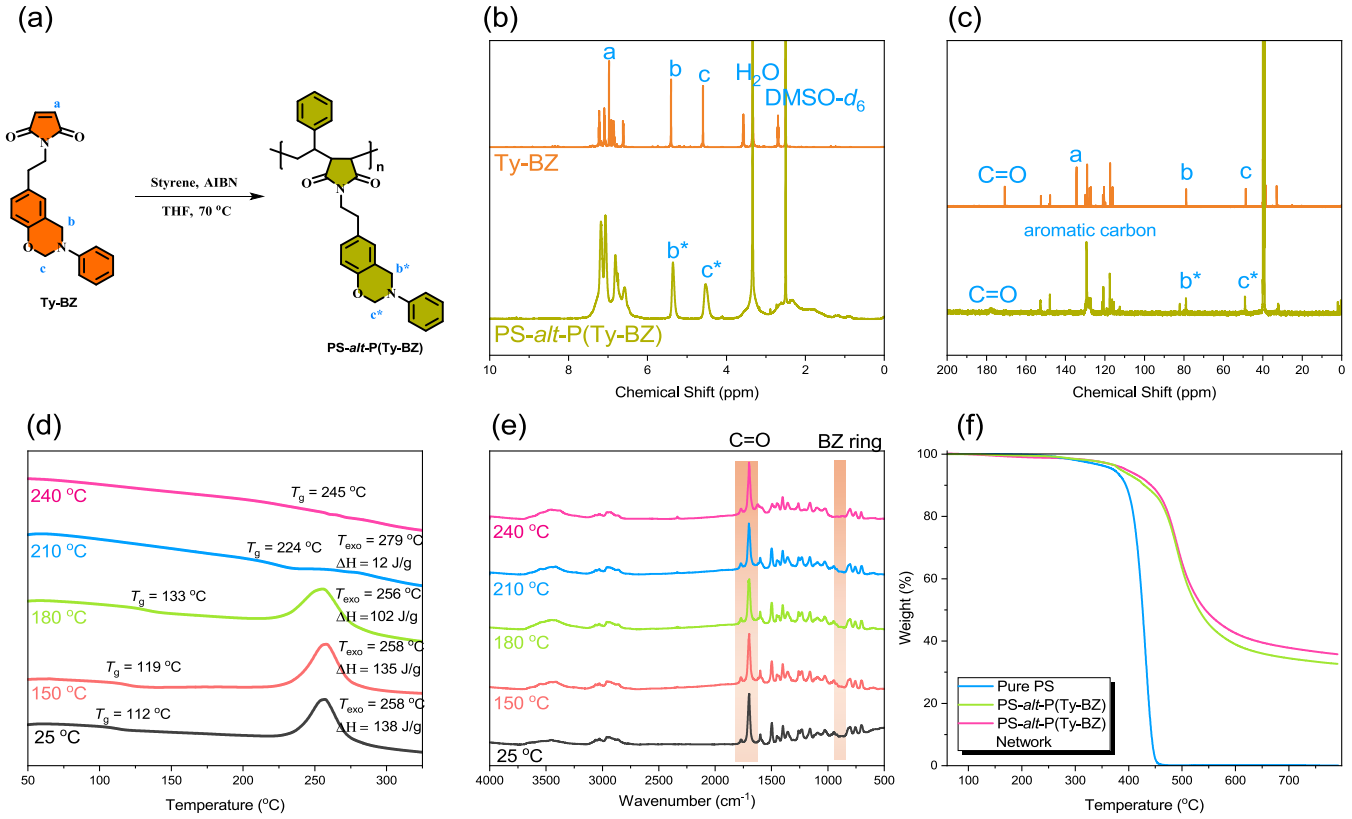

Figure 5. (a) The synthesis of the PS-*alt*-P(Ty-BZ) copolymer by free radical copolymerization from styrene and the Ty-BZ monomer, and their corresponding (b) ^{1}H NMR, (c) ^{13}C NMR, (d–e) DSC, and FTIR analyses under various thermal ROP temperature procedures, and (f) TGA analyses of pure PS, PS-*alt*-P(Ty-BZ) copolymer, and PS-*alt*-P(Ty-BZ) network.

P(Ty-BZ) copolymer with signals at 177.45 and 152.69 ppm due to the C═O and C−OH groups. The C═C unit at 134.14 ppm from the Ty-BZ monomer also disappeared in the PS-*alt*-P(Ty-BZ) copolymer, while the Ar−**C**H$_2$N (*b*) and O-**C**H$_2$N (*c*) carbons remained at 78.73 and 48.41 ppm, respectively. Similarly, the integral area ratio of Ar−**C**H$_2$−N and O−**C**H$_2$−N of PS-*alt*-P(Ty-BZ) copolymer was approximately 1:1 from the ^{1}H NMR spectrum, also suggesting that the benzoxazine ring did not open during free radical copolymerization with the styrene monomer. The ratio of the Ty-BZ segment could be calculated from the oxazine rings compared with the aromatic protons, and the molar percentage of Ty-BZ was determined to be 42.48%, which could be defined as an alternating copolymer by MALDI-TOF mass spectra, as displayed in Figure 6. A nearly perfect alternating copolymer comprising an equal number of Ty-BZ and styrene units[38] was observed; for instance, the 438 g mol^{-1} difference between the *m*/*z* values of 1741.90 (Ty-BZ:S = 4:4) and 2179.3 *m*/*z* (Ty-BZ:S = 5:5) corresponds precisely to the combined molecular weights of one Ty-BZ unit (334 g mol^{-1}) and one styrene unit (104 g mol^{-1}) unit. Predominantly alternating sequences with Ty-BZ:S ratios of *n* − 1:*n*, *n*:*n* and *n*:*n* + 1 were also identified in Figure 6.

Figure 5d,e shows DSC and FTIR analyses of the thermal ROP behavior of the PS-*alt*-P(Ty-BZ) copolymer under various thermal curing temperatures. Pure PS-*alt*-P(Ty-BZ) copolymer exhibited a T_g behavior at 112 °C, which is lower than that of PS-*alt*-P(HPMI-BZ) because of two extra flexible aliphatic CH$_2$ units that increase the free volume and subsequently reduce the T_g behavior. It also displayed a thermal ROP peak at 258 °C with an enthalpy of 138 J/g. With

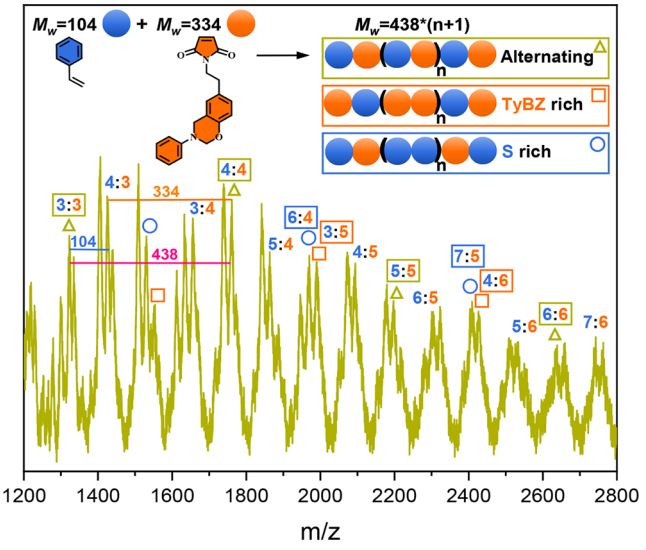

Figure 6. MALDI-TOF mass spectrum of the PS-*alt*-P(Ty-BZ) copolymer.

increasing temperature during ROP, the exothermic peak and enthalpy gradually decreased and then disappeared at 240 °C, indicating complete thermal ROP behavior. In addition, the T_g behavior gradually increased from 112 to 119, 133, 224, and 245 °C as the thermal ROP temperature increases from 25 to 240 °C, respectively. Clearly, the T_g value of the PS-*alt*-P(Ty-BZ) network (T_g = 245 °C) is much higher than that of the PS-*alt*-P(TyHPMI) copolymer (T_g = 146 °C) because of the formation of the network structure, as mentioned previously.

https://doi.org/10.1021/acs.macromol.5c00004
Macromolecules 2025, 58, 6215−6227

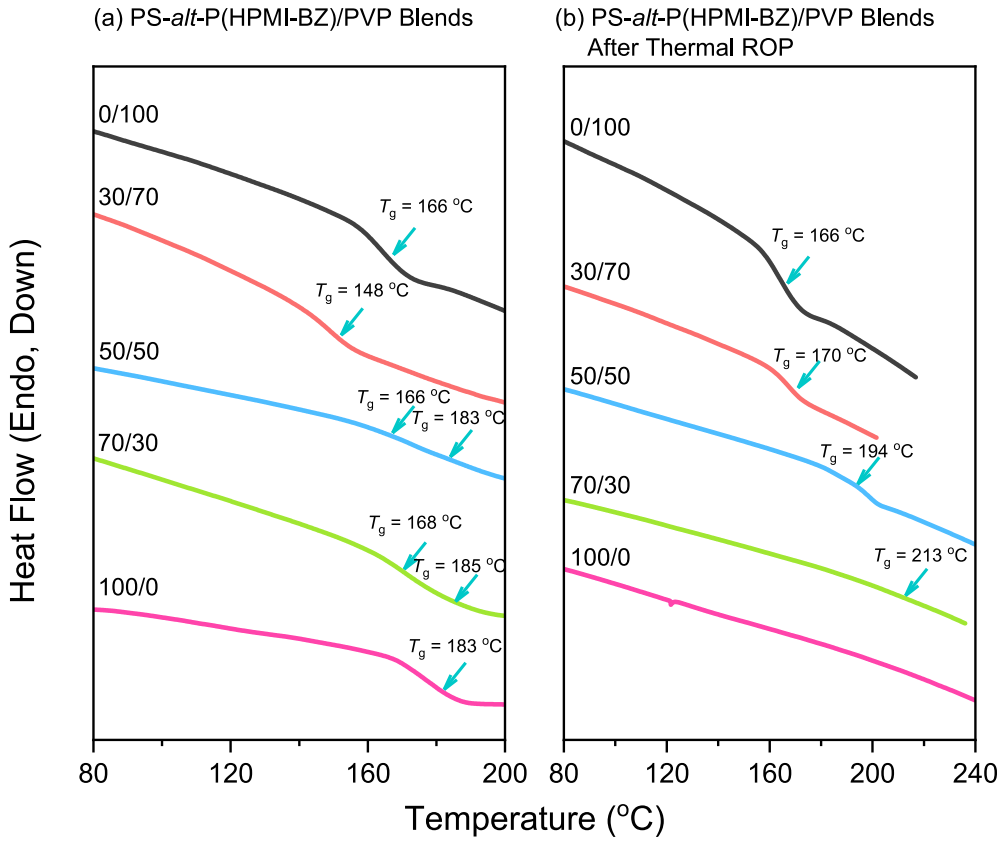

Figure 7. DSC thermograms of various PS-*alt*-P(HPMI-BZ)/PVP blends: (a) first heating scan and (b) second heating scan after thermal ROP.

The absorption of the oxazine ring at 947 cm^{-1} of PS-*alt*-P(Ty-BZ) copolymer decreased as the thermal ROP temperature increased from 25 to 210 °C and totally disappeared after 240 °C, which is consistent with the DSC analyses. Additionally, OH units appeared in the 3700−2500 cm^{-1} region after thermal ROP, and the C═O unit of PS-*alt*-P(HPMI-BZ) copolymer became broadened, indicating the formation of intermolecular hydrogen bonding of C═O---HO groups after thermal ROP to form PS-*alt*-P(Ty-BZ) network, which is similar to PS-*alt*-P (HPMI-BZ) network. Figure 5f displays the TGA analyses of pure PS, PS-*alt*-P(Ty-BZ) copolymer, and the PS-*alt*-P(Ty-BZ) network after thermal ROP at 240 °C. PS-*alt*-P(Ty-BZ) copolymer exhibited a moderate increase in T_{d5} value to 385 °C, with the char yield rising to 32.7 wt %, which is higher than that of pure PS. The PS-*alt*-P(Ty-BZ) network showed a slight increase in T value to 395 °C, with the char yield rising to 35.8 wt %, confirming the formation of the network structure. The thermal stability of the PS-*alt*-P(Ty-BZ) network is lower than that of the PS-*alt*-P(HPMI-BZ) network, as expected, due to the presence of two extra flexible aliphatic CH_2 units. However, the short alkyl CH_2 units could reinforce the increase of acidic TyHPMI units, which could increase the fraction of intermolecular hydrogen bonding between the OH groups of TyHPMI and C═O units of PVP, as investigated previously.[38]

Analyses of PS-*alt*-P(HPMI-Bz) and PS-*alt*-P(Ty-BZ) Copolymers with PVP Blends. In this study, we selected the strong intermolecular hydrogen-bonded acceptor, PVP homopolymer, because of its strongest single hydrogen bonding site of K_A/K_B ratio (approximately 100) when paired with the PVPh homopolymer.[10,36] Figure 7a presents DSC thermal analyses of PS-*alt*-P(HPMI-BZ)/PVP blends with various compositions during the first heating scan after thermal treatment at 180 °C to remove the thermal history of the polymers. The pure PS-*alt*-P(HPMI-BZ) copolymer and pure PVP homopolymer displayed T_g values of 183 and 166 °C, respectively. For the PS-*alt*-P(HPMI-BZ)/PVP = 30/70 blend, the T_g behavior decreased to 148 °C, and the T_g breadth increased to 32 °C, which is higher than that of pure PVP (26 °C) and PS-*alt*-P(HPMI-BZ) (24 °C), suggesting that this binary blend did not possess strong intermolecular interaction. For the PS-*alt*-P(HPMI-BZ)/PVP = 50/50 blend, it exhibited very broad T_g behavior and could be assigned two T_g values, which were further confirmed by the second-derivative differential curve, as shown in Figure S2. These T_g values correspond to PVP at 166 °C and PS-*alt*-P(HPMI-BZ) at 183 °C, suggesting the immiscible behavior of PS-*alt*-P(HPMI-BZ)/PVP blend without strong intermolecular interaction. Similarly, for the PS-*alt*-P(HPMI-BZ)/PVP = 70/30 blend, it exhibited two T_g values at 168 and 185 °C, also indicating the binary immiscible behavior of PS-*alt*-P(HPMI-BZ)/PVP blend. The immiscible PS/PVP binary blend has been widely investigated, as expected, because PS is a hydrophobic polymer and PVP is a hydrophilic polymer.[34,35] In addition, the P(HPMI-BZ) segment contain only a carbonyl group and a benzoxazine ring with polar groups but does not have a strong enough polar interaction to form miscible behavior with the PVP homopolymer. To enhance the miscibility behavior, the second heating scan of the PS-*alt*-P (HPMI-BZ)/PVP blends was conducted, as shown in Figure 7b, after thermal ROP. Clearly, the T_g value increased from 148 to 170 °C, and the T_g breadth decreased from 32 to 29 °C for the PS-*alt*-P(HPMI-BZ)/PVP = 30/70 blend after thermal ROP. More interestingly, as the PS-*alt*-P(HPMI-BZ)/PVP = 50/50 and

https://doi.org/10.1021/acs.macromol.5c00004
Macromolecules 2025, 58, 6215−6227

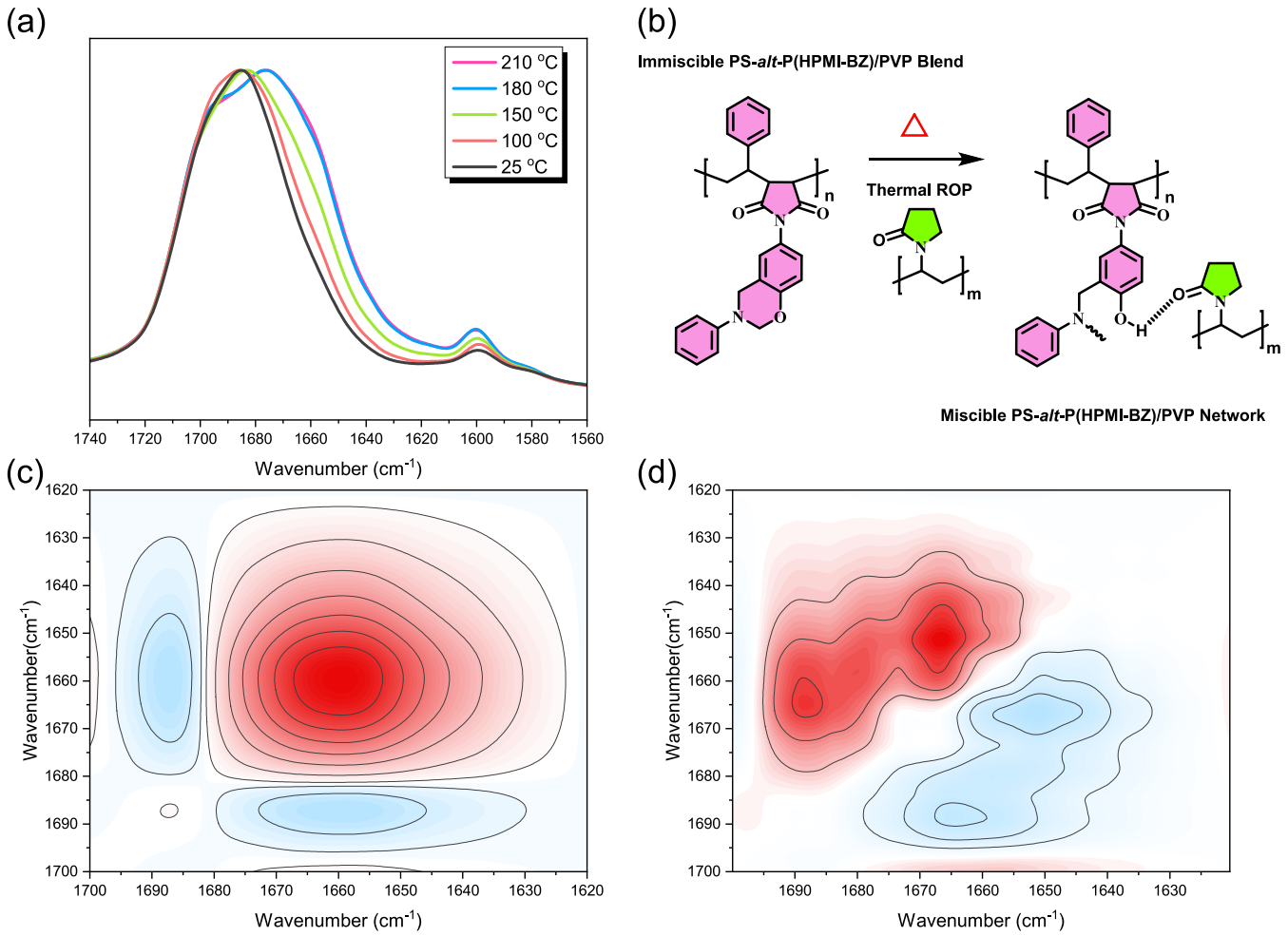

Figure 8. (a) FTIR spectra recorded at various temperature of PS-*alt*-P(HPMI-BZ)/PVP = 50/50 blend, (b) the scheme of intermolecular hydrogen bonding between OH groups of P(HPMI-BZ) after thermal ROP with the C═O groups of PVP, and (c, d) 2D-FTIR spectra showing (c) synchronous and (d) asynchronous correlation spectra.

70/30 blends after thermal ROP, the two T_g values merged into a single T_g value at 194 and 213 °C, respectively. This phenomenon could be explained by two factors: (1) the intramolecular OH---N hydrogen bonding and intermolecular OH---O hydrogen bonding within the PS-*alt*-P(HPMI-BZ) copolymer after thermal ROP, which enhanced the T_g behaviors of PS-*alt*-P(HPMI-BZ) network and (2) the strong intermolecular hydrogen bonding interaction between the OH units of PS-*alt*-P(HPMI-BZ) and C═O units of PVP after thermal ROP to form miscible polymer blends of PS-*alt*-P(HPMI-BZ)/PVP networks.

This result is quite opposite to typical thermoset/thermoplastic blends after thermal curing or thermal polymerization, such as epoxy or phenolic oligomer systems, which is usually observed in the reaction induced phase separation (RIPS) mechanism.[17] In those cases, the oligomers of epoxy or phenolic resin are miscible with thermoplastics such as PVP, PEO, or PCL homopolymers;[18,20,46,47] however, the molecular weight was significantly increased, which induce the entropy change decrease substantially and then increase the Gibbs free energy, leading to macro-phase separation behavior. In addition, the intermolecular interaction between thermoset oligomers and thermoplastic homopolymers might also decrease due to the restricted motion of epoxy or phenolic resin after thermal polymerization. Therefore, the miscibility behavior is strongly dependent on the competition between the enthalpy term from intermolecular hydrogen bonding interactions (a negative term for Gibbs free energy) and the entropy term from thermal polymerization (a positive term for Gibbs free energy). Obviously, the miscible behavior of PS-*alt*-P(HPMI-BZ)/PVP networks is due to the decrease in the enthalpy term from intermolecular hydrogen bonding interactions between the OH units of PS-*alt*-P(HPMI-BZ) and the C═O units of PVP, which favors the increase in the entropy term from thermal ROP.

To confirm the intermolecular hydrogen bonding interaction of PS-*alt*-P(HPMI-BZ)/PVP blends after thermal ROP, the in situ temperature-dependent FTIR spectra were used from room temperature to 210 °C, as shown in Figure 8a. Clearly, the PS-*alt*-P(HPMI-BZ)/PVP = 50/50 blend at room temperature exhibited the free C═O group of PVP at 1683 cm^{-1} and the aromatic ring at 1600 cm^{-1} and 1580 cm^{-1} from PS-*alt*-P(HPMI-BZ) copolymer. After thermal ROP, the C═O absorption of PVP became broad and then a peak appeared at 1675 cm^{-1} and a shoulder at 1660 cm^{-1}, both corresponding to the intermolecular dipole−dipole and hydrogen bonding interaction[20] between OH units of PS-*alt*-P(HPMI-BZ) and C═O units of PVP after thermal ROP, as shown in Figure 8b. To understand the changes in the intermolecular hydrogen bonding interaction of the PS-*alt*-P(HPMI-BZ)/PVP blends,

https://doi.org/10.1021/acs.macromol.5c00004
Macromolecules 2025, 58, 6215−6227

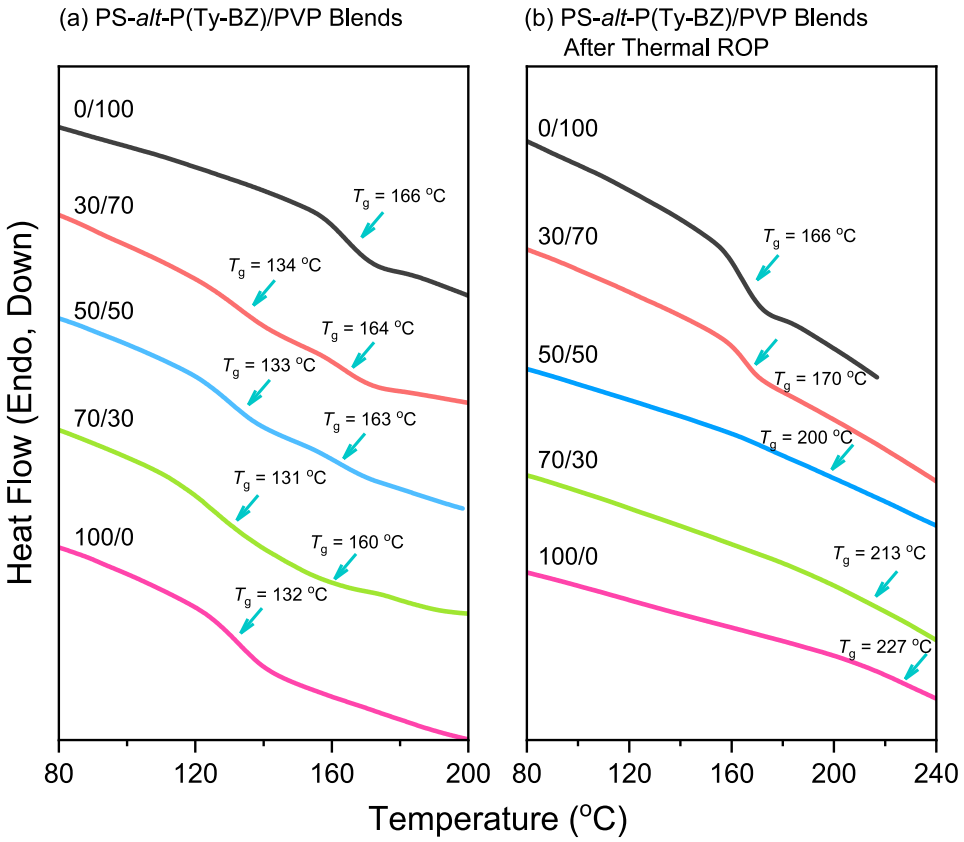

Figure 9. DSC thermograms of various PS-*alt*-P(Ty-BZ)/PVP blends: (a) first heating scan and (b) second heating scan after thermal ROP.

Scheme 1. The Synthesis of Benzoxazine Monomers, Alternating Copolymers and the Possible RIM Behavior in Binary Polymer Blends

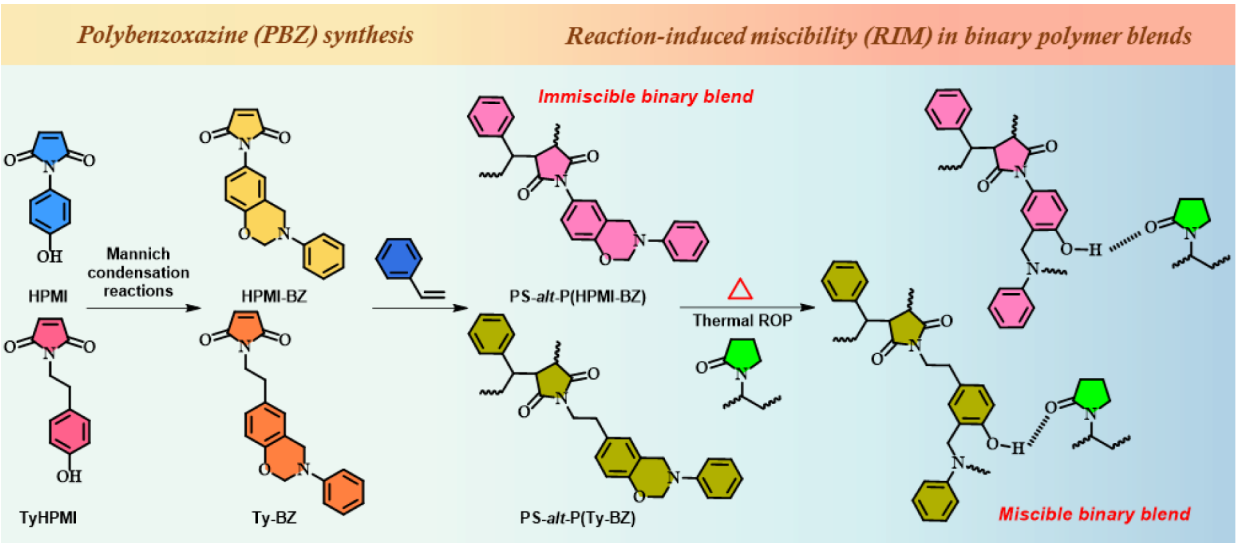

the 2D-FTIR correlation maps[48,49] were employed, as shown in Figure 8c,d. The synchronous correlation spectrum, as displayed in Figure 8c, presents two major autopeaks (red colors) at 1683 cm^{-1} and 1660 cm^{-1}, corresponding to free and hydrogen bonded C═O units of PVP as mentioned in 1D-FTIR analysis, respectively. Two negative cross-peaks (blue color) were observed between the free C═O unit (1683 cm^{-1}) and the hydrogen bonded C═O unit (1660 cm^{-1}), indicating a change in opposite directions as the temperature increased. In addition, the signal of the hydrogen bonded C═O unit would be affected by temperature perturbation earlier than the free C═O unit, as shown in Figure 8d by the asynchronous correlation spectrum, as expected.[48,49]

Now we turn our attention to the PS-*alt*-P(Ty-BZ)/PVP blends, where the short alkyl CH_2 units could reinforce the increase of acidic Ty-BZ units, which could increase the fraction of intermolecular hydrogen bonding between the OH groups of Ty-BZ and C═O units of PVP after thermal ROP,

https://doi.org/10.1021/acs.macromol.5c00004
Macromolecules 2025, 58, 6215−6227

as mentioned previously.[38] Figure 9a shows DSC thermograms of PS-*alt*-P(Ty-BZ)/PVP blends with various compositions during the first heating scan after thermal treatment at 180 °C. The pure PS-*alt*-(Ty-BZ) copolymer displayed a T_g value of 132 °C, which is much lower than the pure PS-*alt*-P(HPMI-BZ) (T_g = 183 °C), as expected due to the presence of two extra flexible aliphatic CH_2 units that increase free volume and subsequently reduce the T_g behavior. All binary PS-*alt*-P(Ty-BZ)/PVP blends display two T_g values, which can also be confirmed by the second-derivative differential curve, as shown in Figure S3. The relatively lower T_g value (131−134 °C) corresponds to PS-*alt*-P(Ty-BZ) copolymer domain, while the relatively higher T_g value (160−164 °C) corresponds to the pure PVP homopolymer domain, indicating the immiscible behavior of PS-*alt*-P(Ty-BZ)/PVP blends, as expected. However, after thermal ROP of PS-*alt*-P(Ty-BZ)/PVP blends, as displayed in Figure 9b, the two T_g values merged into a single T_g value of 170, 200, and 213 °C for PS-*alt*-P(Ty-BZ)/PVP = 30/70, 50/50, and 70/30, respectively.

All results provide the miscible behavior of PS-*alt*-P(Ty-BZ)/PVP networks because of the strong intermolecular hydrogen bonding interaction between the OH units of PS-*alt*-P(Ty-BZ) and the C═O units of PVP, which favored an increase in the entropy term during thermal ROP. This behavior is similar with PS-*alt*-P(HPMI-BZ)/PVP network. Furthermore, the T_g behavior of PS-*alt*-P(Ty-BZ)/PVP networks is close to or even slightly higher than that of PS-*alt*-P(HPMI-BZ)/PVP networks across all blend compositions. Even though pure PS-*alt*-P(Ty-BZ) exhibited a lower T_g value compared to PS-*alt*-P(HPMI-BZ), the self-association hydrogen bonding of OH---OH and OH---O═C units in poly(S−alt−TyBZ) was reduced because the short alkyl CH_2 units reinforced the increase of acidic TyBZ units. This reduction in self-association decreased the K_B value, further increased the K_A/K_B ratio in binary blends, and ultimately enhanced the T_g behavior. Furthermore, compared with the typical BA-a type benzoxazine blending with PVP homopolymer, the T_g behavior is located at approximately 180−190 °C for all blend compositions after thermal ROP[20] and thus the PS-*alt*-P(HPMI-BZ)/PVP and PS-*alt*-P(Ty-BZ)/PVP blends exhibited significantly improved thermal properties. Scheme 1 summarizes the synthesis of all the benzoxazine monomers, PS-*alt*-P(HPMI-BZ) and PS-*alt*-P(Ty-BZ) alternating copolymers, and the possible reaction-induced miscibility behavior with PVP binary polymer blends in this study.

Overall, these result indicate that the PS−*alt*−P(Ty-BZ) copolymer can more effectively enhance both the thermal properties and miscibility behavior when blended with the PVP homopolymer, even though the T_g value of pure PS-*alt*-P(Ty-BZ) is much lower than that of the pure PS-*alt*-P(HPMI-BZ) copolymer.

CONCLUSIONS

This study has demonstrated a novel approach to achieving reaction-induced miscibility (RIM) in traditionally immiscible polymer blends by leveraging intermolecular hydrogen bonding through the design and synthesis of PS-*alt*-P(HPMI-BZ) and PS-*alt*-P(Ty-BZ) copolymers, allowing for enhanced miscibility with PVP homopolymer after thermal ROP. The successful synthesis of novel benzoxazine monomers and their alternating copolymers was confirmed through advanced characterization techniques, such as NMR, FTIR, DSC, TGA, and MALDI-TOF, showcasing their structural integrity and thermal stability. The thermal ROP of the benzoxazine units introduced phenolic hydroxyl functional groups that formed strong intermolecular hydrogen bonds with the carbonyl groups of PVP, enabling miscibility in otherwise immiscible PS/PVP systems, which is confirmed by a single T_g value based on DSC analyses, confirming the miscibility induced by the specific intermolecular interactions based on 1D and 2D-FTIR analyses. This research highlights the potential of RIM as a transformative strategy for developing advanced polymer blends with tailored properties. By designing copolymers with strategic functional groups, it is possible to overcome traditional thermodynamic challenges and achieve homogeneous polymer blends suitable for potential applications. These findings also pave the way for further exploration of RIM in other polymer systems, enabling innovative materials with enhanced mechanical, thermal, and functional properties.

ASSOCIATED CONTENT

Supporting Information

The Supporting Information is available free of charge at https://pubs.acs.org/doi/10.1021/acs.macromol.5c00004.

Characterization methods, GPC analyses of PS-*alt*-P(HPMI-BZ) and PS-*alt*-P(Ty-BZ) copolymers, and second-derivative differential DSC curves of PS-*alt*-P(HPMI-BZ)/PVP and PS-*alt*-P(Ty-BZ)/PVP binary blends (PDF)

AUTHOR INFORMATION

Corresponding Author

Shiao-Wei Kuo − *Department of Materials and Optoelectronic Science, Center for Functional Polymers and Supramolecular Materials, National Sun Yat-Sen University, Kaohsiung 80424, Taiwan;* orcid.org/0000-0002-4306-7171; Email: kuosw@faculty.nsysu.edu.tw

Authors

Tzu-Ling Ma − *Department of Materials and Optoelectronic Science, Center for Functional Polymers and Supramolecular Materials, National Sun Yat-Sen University, Kaohsiung 80424, Taiwan*

Wei-Ting Du − *Department of Materials and Optoelectronic Science, Center for Functional Polymers and Supramolecular Materials, National Sun Yat-Sen University, Kaohsiung 80424, Taiwan*

Yang-Chin Kao − *Department of Materials and Optoelectronic Science, Center for Functional Polymers and Supramolecular Materials, National Sun Yat-Sen University, Kaohsiung 80424, Taiwan*

Mohamed Gamal Mohamed − *Department of Materials and Optoelectronic Science, Center for Functional Polymers and Supramolecular Materials, National Sun Yat-Sen University, Kaohsiung 80424, Taiwan;* orcid.org/0000-0003-0301-8372

Complete contact information is available at: https://pubs.acs.org/10.1021/acs.macromol.5c00004

Author Contributions

The manuscript was written through contributions of all authors.

Notes

The authors declare no competing financial interest.

https://doi.org/10.1021/acs.macromol.5c00004
Macromolecules 2025, 58, 6215−6227

■ ACKNOWLEDGMENTS

This study was financially supported by the National Science and Technology Council, Taiwan, under contracts NSTC 113-2218-E-110-004 and 113-2223-E-110-001.

■ REFERENCES

(1) Hirai, T.; Amano, K.; Onochi, Y.; Inoue, Y. Superior hygrothermal resistance and interfacial adhesion by ternary thermoplastic polymer blend matrix for carbon fiber composite. *Compos. A Appl. Sci. Manufact.* **2021**, *144*, 106338.
(2) Alkhodairi, H.; Russell, S. T.; Pribyl, J.; Benicewicz, B. C.; Kumar, S. K. Compatibilizing Immiscible Polymer Blends with Sparsely Grafted Nanoparticles. *Macromolecules* **2020**, *53*, 10330−10338.
(3) Lyu, S. P.; Sparer, R.; Hobot, C.; Dang, K. Adjusting drug diffusivity using miscible polymer blends. *J. Controlled Release* **2005**, *102*, 679−687.
(4) Tang, H.; Chao, G.; Gao, J.; Shang, Y.; Li, N.; Geng, K. Tailoring of microporosity of Tröger's base (TB) high temperature proton exchange membrane by miscible polymer blending. *J. Power Sources* **2023**, *565*, 232868.
(5) Li, Y.; Zhang, Y.; Wu, B.; Pang, S.; Yuan, X.; Duan, C.; Huang, F.; Cao, Y. High-efficiency P3HT-based all-polymer solar cells with a thermodynamically miscible polymer acceptor. *Sol. RRL* **2022**, *6*, 2200073.
(6) Kamal, M. R.; Utracki, L. A.; Mirzadeh, A. Rheology of Polymer Alloys and Blends Reference work entry First Online: 01 January 2014. In *Polymer Blends Handbook*; Springer, 2014, pp. 725−873. DOI: .
(7) Kuo, S. W. Hydrogen-bonding in polymer blends. *J. Polym. Res.* **2008**, *15*, 459−486.
(8) Huang, C. C.; Du, M. X.; Zhang, B. Q.; Liu, C. Y. Glass transition temperatures of copolymers: Molecular origins of deviations from the linear relation. *Macromolecules* **2022**, *55*, 3189−3200.
(9) Kulshreshtha, A.; Hayward, R. C.; Jayaraman, A. Impact of Composition and Placement of Hydrogen-Bonding Groups along Polymer Chains on Blend Phase Behavior: Coarse-Grained Molecular Dynamics Simulation Study. *Macromolecules* **2022**, *55*, 2675−2690.
(10) Coleman, M. M.; Painter, P. C. Hydrogen Bonded Polymer Blends. *Prog. Polym. Sci.* **1995**, *20*, 1−59.
(11) He, Y.; Zhu, B.; Inoue, Y. Hydrogen Bonds in Polymer Blends. *Prog. Polym. Sci.* **2004**, *29*, 1021−1051.
(12) Kuo, S. W. *Hydrogen Bonding in Polymer Materials*; John Wiley & Sons: Hoboken, NJ, 2018.
(13) Chen, W. C.; Kuo, S. W.; Jeng, U. S.; Chang, F. C. Self-assembly through competitive interactions of miscible diblock copolymer/homopolymer blends: Poly (vinylphenol-b-methyl methacrylate)/poly(vinylpyrrolidone) blend. *Macromolecules* **2008**, *41*, 1401−1410.
(14) Kuo, S. W.; Lin, C. L.; Chang, F. C. Phase behavior and hydrogen bonding in ternary polymer blends of phenolic resin/poly (ethylene oxide)/poly (ε-caprolactone). *Macromolecules* **2002**, *35*, 278−285.
(15) Mathis, E.; Michon, M. L.; Billaud, C.; Vergelati, C.; Clarke, N.; Jestin, J.; Long, D. R. Controlling the Morphology in Epoxy/Thermoplastic Systems. *ACS Appl. Polym. Mater.* **2022**, *4*, 2091−2104.
(16) Voleppe, Q.; Ballout, W.; Van Velthem, P.; Bailly, C.; Pardoen, T. Enhanced fracture resistance of thermoset/thermoplastic interfaces through crack trapping in a morphology gradient. *Polymer* **2021**, *218*, 123497.
(17) Inoue, T. Reaction-induced phase decomposition in polymer blends. *Prog. Polym. Sci.* **1995**, *20*, 119−153.
(18) Chen, J. L.; Chang, F. C. Phase Separation Process in Poly(ε-caprolactone)−Epoxy Blends. *Macromolecules* **1999**, *32*, 5348−5356.
(19) Aravind, I.; Eichhorn, K. J.; Komber, H.; Jehnichen, D.; Zafeiropoulos, N. E.; Ahn, K. H.; Grohens, Y.; Stamm, M.; Thomas, S. A Study on Reaction-Induced Miscibility of Poly(trimethylene terephthalate)/Polycarbonate Blends. *J. Phys. Chem. B* **2009**, *113*, 1569−1578.
(20) Su, Y. C.; Kuo, S. W.; Yei, D. R.; Xu, H.; Chang, F. C. Thermal Properties and Hydrogen Bonding in Polymer Blend of Polybenzoxazine/Poly(*N*-Vinyl-2-Pyrrolidone). *Polymer* **2003**, *44*, 2187−2191.
(21) Otsuka, H.; Aotani, K.; Higaki, Y.; Takahara, A. Polymer Scrambling: Macromolecular Radical Crossover Reaction Between The Main Chains Of Alkoxyamine-Based Dynamic Covalent Polymers. *J. Am. Chem. Soc.* **2003**, *125*, 4064−4065.
(22) Yang, Y.; Ding, X.; Urban, M. W. Chemical and Physical Aspects of Self-Healing Materials. *Prog. Polym. Sci.* **2015**, *49*, 34−59.
(23) Kao, Y. C.; Ku, Y. H.; Mohamed, M. G.; Su, W. H.; Kuo, S. W. Microphase Separation Transformation in Bio-Based Benzoxazine/Phenolic/PEO-*b*-PCL Diblock Copolymer Mixtures Induced by Transesterification Reaction. *Macromolecules* **2025**, *58*, 585−600.
(24) Lu, Y.; Liu, J.; Zhao, W.; Zhang, K. Bio-benzoxazine structural design strategy toward highly thermally stable and intrinsically flame-retardant thermosets. *Chem. Eng. J.* **2023**, *457*, 141232.
(25) Wang, W.; Liu, H.; Pei, L.; Liu, H.; Wang, M.; Li, S.; Wang, Z. Modified polybenzoxazine and carbon fiber surface with improved mechanical properties by introducing hydrogen bonds. *Eur. Polym. J.* **2023**, *182*, 111717.
(26) Wang, C. F.; Su, Y. C.; Kuo, S. W.; Huang, C. F.; Sheen, Y. C.; Chang, F. C. Low-Surface-Free-Energy Materials Based on Polybenzoxazines. *Angew. Chem., Int. Ed.* **2006**, *45*, 2248−2251.
(27) Wang, C. F.; Chiou, F. H.; Ko, F. H.; Chen, J. K.; Chou, C. T.; Huang, C. F.; Kuo, S. W.; Chang, F. C. Polybenzoxazine as a mold-release agent for nanoimprint lithography. *Langmuir* **2007**, *23*, 5868−5871.
(28) Heyman, E.; Pearce, M.; Ishida, H. Synthesis of Water-Soluble, Intrinsically Flame-Retardant Benzoxazine Based on Renewable, Natural Resources. *ACS Sustainable Chem. Eng.* **2025**, *13*, 4182−4191.
(29) Yang, R.; Zhang, K. Synthesis of Isoliquiritgenin-Based Bio-Benzoxazine and Its Role of Latent Curing Agent for Achieving High-Performance Epoxy Thermosetting Systems. *Mater. Today Commun.* **2025**, *45*, 112374.
(30) Song, J.; Liang, H.; Cao, Y.; Wang, M.; Wang, Z. Advancing coatings with polybenzoxazines: insights into molecular design, synthesis, and modification. *J. Mater. Chem. A* **2024**, *12*, 9094−9111.
(31) Chen, W. C.; Kuo, S. W. Ortho-Imide and Allyl Groups Effect on Highly Thermally Stable Polybenzoxazine/Double-Decker-Shaped Polyhedral Silsesquioxane Hybrids. *Macromolecules* **2018**, *51*, 9602−9612.
(32) Mohamed, M. G.; Kuo, S. W. Crown Ether-Functionalized Polybenzoxazine for Metal Ion Adsorption. *Macromolecules* **2020**, *53*, 2420−2429.
(33) Ishida, H.; Froimowicz, P. *Advanced and Emerging Polybenzoxazine Science and Technology*; Elsevier: Amsterdam, 2017.
(34) Shen, X.; Cao, L.; Liu, Y.; Dai, J.; Liu, X.; Zhu, J.; Du, S. How does the hydrogen bonding interaction influence the properties of polybenzoxazine? An experimental study combined with computer simulation. *Macromolecules* **2018**, *51*, 4782−4799.
(35) Mukherjee, S.; Lochab, B. Hydrogen Bonding-Guided Strategies for Thermal Performance Modulation in Biobased Oxazine Ring-Substituted Benzoxazine Thermosets. *Macromolecules* **2024**, *57*, 1795−1807.
(36) Yang, R.; Li, N.; Evans, C. J.; Yang, S.; Zhang, K. Phosphaphenanthrene-functionalized benzoxazines bearing intramolecularly hydrogen-bonded phenolic hydroxyl: synthesis, structural characterization, polymerization mechanism, and property investigation. *Macromolecules* **2023**, *56*, 1311−1323.
(37) Ejaz, M.; Mohamed, M. G.; Kuo, S. W. Benzoxazine-linked polyhedral oligomeric silsesquioxane: 3D porous organic-inorganic polymer for improved CO_2 capture and supercapacitor performance. *J. Taiwan Inst. Chem. Eng.* **2025**, *106098*, 106098.
(38) Wu, K. U.; Lu, S. Y. Preferential Partition of Nanowires in Thin Films of Immiscible Polymer Blends. *Macromol. Rapid Commun.* **2006**, *27*, 424−429m.

https://doi.org/10.1021/acs.macromol.5c00004
Macromolecules 2025, 58, 6215−6227

(39) Kang, H.; Lee, S. H.; Kim, S.; Char, K. Dewetting and Layer Inversion of Inverted PVP/PS Bilayer Films. *Macromolecules* **2003**, *36*, 8579−8583.
(40) Kuo, S. W.; Chang, F. C. Studies of Miscibility Behavior and Hydrogen Bonding in Blends of Poly(vinylphenol) and Poly-(vinylpyrrolidone). *Macromolecules* **2001**, *34* (15), 5224−5228.
(41) Du, W. T.; Orabi, E. A.; Mohamed, M. G.; Kuo, S. W. Inter/intramolecular hydrogen bonding mediate miscible blend formation between near−perfect alternating Poly (styrene−*alt*−hydroxyphenyl-maleimide) copolymers and Poly (vinyl pyrrolidone. *Polymer* **2021**, *219*, 123542.
(42) Ma, T. L.; Du, W. T.; Kuo, S. W. Design and mediated hydrogen bonding strength of Poly (styrene−*alt*−*N*−(ethyl−4−hydroxyphenyl) maleimide) copolymer to enhance miscibility with hydrogen bonded acceptor homopolymers. *Polymer* **2024**, *311*, 127574.
(43) EL-Mahdy, A. F. M.; Kuo, S. W. Direct synthesis of poly(benzoxazine imide) from an ortho−benzoxazine: Its thermal conversion to highly cross−linked polybenzoxazole and blending with poly (4−vinylphenol). *Polym. Chem.* **2018**, *9*, 1815−1826.
(44) Mohamed, M. G.; Li, C. J.; Khan, M. A. R.; Liaw, C. C.; Zhang, K.; Kuo, S. W. Formaldehyde-Free Synthesis of Fully Bio-Based Multifunctional Bisbenzoxazine Resins from Natural Renewable Starting Materials. *Macromolecules* **2022**, *55*, 3106−3115.
(45) Abuzeid, H. R.; El-Mahdy, A. F. M.; Ahmed, M. M. M.; Kuo, S. W. Triazine-Functionalized Covalent Benzoxazine Framework for Direct Synthesis of N-Doped Microporous Carbon. *Polym. Chem.* **2019**, *10*, 6010−6020.
(46) Li, J. G.; Lin, Y. D.; Kuo, S. W. From microphase separation to self-organized mesoporous phenolic resin through competitive hydrogen bonding with double-crystalline diblock copolymers of poly(ethylene oxide-b-ε-caprolactone). *Macromolecules* **2011**, *44*, 9295−9309.
(47) EL-Mahdy, A. F. M.; Yu, T. C.; Mohamed, M. G.; Kuo, S. W. Secondary Structures of Polypeptide-Based Diblock Copolymers Influence the Microphase Separation of Templates for the Fabrication of Microporous Carbons. *Macromolecules* **2021**, *54*, 1030−1042.
(48) Noda, I. Two-Dimensional Infrared Spectroscopy. *J. Am. Chem. Soc.* **1989**, *111*, 8116−8118.
(49) Mantala, K.; Crespy. D. Poly(urea-urethane) Elastomers Showing Autonomous Healing at Room Temperature. *Macromolecules* **2023**, *56*, 7332−7343.

https://doi.org/10.1021/acs.macromol.5c00004
Macromolecules 2025, 58, 6215−6227